A Study on the Finite Element Preprocessing for the Analysis and Design with Discontinuous Composites

Hong Gun Kim*

(*Received August 6, 1997*)

A strategy of finite element (FE) preprocessing of discontinuous fiber or whisker reinforced composite materials for mechanical analysis and design has been treated in this paper. The procedures were based on the calculation of the error in energy norm for global convergence and the traction differential approach at the fiber/matrix interface for local convergence. The mesh refinement strategy was intended to the h-based generalized approach using the elongated element at the fiber/matrix interface, which yields significantly different patterns from those obtained by conventional mesh refinement procedures. This difference may have a critical bearing on the subsequent thermo-mechanical properties predicted by the finite element analysis (FEA). It was found that the FE mesh design of adequate element aspect ratio at the fiber/matrix interface results in a much more rapid computational convergence rate than that obtained by the conventional approach.

Key Words: Error Energy Norm, Global Convergence, Local Convergence, h-Version, p-Version, Element Aspect Ratio, *a posteriori* Error Estimates, Discontinuous Composite Material, C^0 Continuity, L_2 Norm

Nomencalture

$u=u(r, z)$: Radial displacement
$w=w(r, z)$: Axial displacement
ε : Strain
σ : Stress
α : Coefficient of thermal expansion
f : Body force
R : Residual
N : Weighting function
Ω : Domain
Γ : Boundary
$[K]$: Stiffness matrix
$[B]$: Strain-displacement matrix
$[D]$: Stress-strain matrix
$\{F\}$: Force vector
$\{d\}$: Displacement vector
M : Number of elements
$\{\bar{\sigma}^*\}_n$: Smoothed stress vector at node n
$\{\hat{\sigma}\}_n$: Unaveraged stress vector at node n
$\{\sigma^*\}_n$: Improved stress vector at node n
$\| e_\sigma \|$: Energy norm
E : Normalized percent error
T : Traction

Subscripts

r : Radial direction
θ : Hoop direction
z : Axial direction
m : Matrix
f : Fiber
i : Node

Superscripts

e : Element component
n : Unit outward normal to the boundary

* Department of Mechanical Engineering, Jeonju University, 1200 Hyojadong 3 Ga, Wansangu, Jeonju 560-759, Korea.

1. Introduction

The finite element analysis (FEA) offers a

rigorous and versatile approach in the composite analysis and design. While FEA usually gives a good result, the application of FEA to composite requires careful attention to the geometry of the optimum mesh refinement. Intrinsically, FEA involves the geometric and mathematical discretization of a continuum into a FE mesh which is reflected by a discretization error in the analysis. Hence, *a posteriori* error estimations (Strang and Fix, 1973) for the FEA solution have become very essential and are currently an active research area. These a posteriori error estimates are then taken as a basis for adaptively refining the mesh. The meshes can be locally refined based on local error determinators, uniformally refined based on a global measure of the discretization error, or refined by a combination of local and global error measures.

Babuska and Rheinboldt (1978) have offered mathematically more rigorous, residual-based approaches to error analysis. They derived error bounds for the energy norm of the error based on the residual of the differential equation. Element error indicators were introduced as a means of determining which elements must be refined. Mesh optimality is based on achieving uniform error distribution for all elements. Subsequent work continued to develop residual-based error estimators and associated adaptive mesh refinement schemes (Babuska and Miller, 1984, Rheinboldt, 1985).

Other residual-based methods include the work of Kelly *et al.* (1983). In an attempt to reduce the computational burden involved in residual-based error estimates, the authors proposed the use of special hierarchical shape functions. The hierarchical shape functions essentially permit efficient p-based error estimates. However, a common fundamental problem of all residual-based methods has been the difficulty of correlating the residual, as measured by an integral norm, to the pointwise error in either the primary displacement variable or its derivatives, such as strains and stresses.

On the other hand, Zienkiewicz and Zhu (1987) have derived a new stress-based error estimator and associated adaptivity algorithm. This method (hereafter referred to as the ZZ method) involved obtaining a global least squares fit of the discontinuous (C^{-1} continuous) FE stress field with a C^0 continuous stress field. The latter stress field is taken as an approximation to the true stress field, and the difference between the two tensor fields, as measured by the energy or L_2 norm, represents an estimate of the discretization error. The authors invoke the asymptotic convergence rate of displacement-based finite elements to correlate the norm of the error in the element stress field to the FE size, thereby deriving an adaptive element sizing function for the new mesh.

Ainsworth *et al.* (1989) have shown that the ZZ error estimator is effective and asymptotically exact provided that the exact stress boundary conditions are imposed on the higher other stress field. However, imposition of exact stress boundary conditions for general multi-dimensional problems, while straightforward, involves additional computations. *Cauchy* stress components must be transformed to boundary-based normal/tangential coordinate systems for all boundary elements. Moreover, the order of the system of equations generated by the least squares fit problem is, in general, larger than the original FE system of equations. Thus, the algorithm is computationally intensive, unless the coefficient matrix for the least squares fit problem is diagonalized as recommended by Zienkiewicz and Zhu (1987). The effect of this diagonalization or lumping of the coefficient matrix on the effectiveness, accuracy and convergence properties of the algorithm was not explored by Ainsworth *et al.* (1989).

On the other hand, Ohtsubo and Kitamura (1990) put forward a method by which an element-by-element error analysis can be carried out using an isoparametric element having an interpolation function one order higher than the original element and imposing self-equilibrium conditions in individual elements. Zhu and Zienkiewiez (1990) also showed that error estimations based on higher order approximations of the gradient field can be directly related to the residual-based error estimator proposed and analysed

by Babuska and Rheinboldt (1978).

Recently, Grosse *et al.* (1992) proposed a new *a posteriori* FE error estimator based on *von* Mises or effective stress function and on a new concept of mesh optimality. In their study, the discretization error is estimated by the L2 norm of the difference between FE von Mises stress function and an improved "smoothed" von Mises stress function. The element error measure is shown to have a distortional energy interpretation. The mesh adaptivity algorithm is based on imposing a nonuniform distribution of allowable error, as measured by the element's L_2 error norm, based on the element's stress state. In this manner, the desired solution accuracy in the mesh is permitted to vary according to the relative stress distribution with the highest solution accuracy required in the highest stressed regions and the minimum solution accuracy required in the lowest stressed regions.

The above procedures have yet to be generalized and extended to the case of fiber or whisker reinforced "non-homogeneous" composite materials. In discontinuous composite systems, because the stress field is highly sensitive to the geometry of fiber and cell, i. e. fiber and/or cell aspect ratio, the mesh geometry is critical. In such composites, it is presented that FE meshes of the appropriately elongated elements are desirable near the fiber/matrix interface unless element aspect ratios are too large. In this case, the automatic free mesh generation shows some difficulty when combining the *Regular Element* (RE) far from the fiber/matrix interface, which has a nearly uniform element aspect ratio, with highly *Elongated Element* (EE) at the fiber/matrix interface having fairly large element aspect ratio. Most of previous FE error estimation studies used the local error energy norm for computing the local error. However, short fiber or whisker reinforced composites usually have sharp corners at the inter-material boundary that can produce a singularity and a lack of C^0 continuity across fiber/matrix interface (Needleman and Nutt, 1986 ; Nutt and Duva, 1987). Again, this method has limitations for short fiber or whisker reinforced composites. Thus far, it is needed to establish a new local error parameter that provides an optimal convergence condition.

In this paper, a mesh refinement procedure is presented using a new local error parameter for a discontinuous fiber reinforced composite. It includes the previous global error energy norm parameters as well as a new local error parameter based on a normal traction discontinuity. The error criteria based on energy have been evaluated in the fiber and matrix separately for a global convergence because C^0 continuity invalidates this energy approach in the fiber/matrix interface region. A normal traction differential approach was applied at the interfacial nodes in order to predict the local near-interface mesh quality. It was found that appropriately high element aspect ratios near the fiber/matrix interface are very efficient for modeling with the h-based FE mesh refinement in discontinuous fiber or whisker reinforced composites. Furthermore, this phenomenon was also explained by the concept of "characteristic element length" depicted by logarithmic plotting and it demonstrates that there is nothing really magical.

2. Governing Equations and FE Formulations

The governing equations and the Galerkin FEA formulations for the axisymmetric linear isotropic elasticity used here are presented in this section. Note that, although on a macroscopic level short fiber composites are anisotropic material at this micromechanical model, we can assume isotropic material behavior for the fiber itself and for the matrix itself.

Let $u=u(r,\ z)$ and $w=w(r,\ z)$ represent the radial and axial (fiber direction) components of the displacement field, respectively. The strain-displacement relationships in linear axisymmetric elasticity are :

$$\{\varepsilon\}\begin{Bmatrix}\varepsilon_r\\ \varepsilon_\theta\\ \varepsilon_z\\ \gamma_{rz}\end{Bmatrix}=\begin{Bmatrix}\dfrac{\partial u}{\partial r}\\ \dfrac{u}{r}\\ \dfrac{\partial w}{\partial z}\\ \dfrac{\partial u}{\partial z}+\dfrac{\partial w}{\partial r}\end{Bmatrix} \tag{1}$$

where ε_θ is the hoop strain. The constitutive relations for isotropic axisymmetric elasticity with initial strains are

$$\{\sigma\}=\begin{Bmatrix}\sigma_r\\ \sigma_\theta\\ \sigma_z\\ \tau_{rz}\end{Bmatrix}=[D]\left(\begin{Bmatrix}\varepsilon_r\\ \varepsilon_\theta\\ \varepsilon_z\\ \gamma_{rz}\end{Bmatrix}-\{\varepsilon_o\}\right) \tag{2}$$

where

$$[D]=\frac{E}{(1+\nu)(1-2\nu)}\begin{bmatrix}1-\nu & \nu & \nu & 0\\ \nu & 1-\nu & \nu & 0\\ \nu & \nu & 1-\nu & 0\\ \nu & \nu & \nu & \frac{1}{2}-\nu\end{bmatrix} \tag{3}$$

and the thermally-induced initial strain tensor, as is the case here, has the form

$$\{\varepsilon_o\}=\alpha\,\Delta T\begin{Bmatrix}\varepsilon_r\\ \varepsilon_\theta\\ \varepsilon_z\\ \gamma_{rz}\end{Bmatrix} \tag{4}$$

where α is the material coefficient of thermal expansion (CTE) and ΔT is the temperature change of the material relative to the strain-free reference temperature.

Finally, we have the differential equilibrium conditions for axisymmetric elasticity as follows :

$$\begin{aligned}&\sigma_{r,r}+\frac{1}{r}(\sigma_r-\sigma_\theta)+\tau_{rz,z}+f_r=0\\ &\sigma_{z,z}+\tau_{rz,r}+\frac{1}{r}\tau_{rz}+f_z=0\end{aligned}\qquad (r,\ z)\in\Omega \tag{5}$$

where f_r and f_z are body forces. The boundary equilibrium conditions are

$$\begin{aligned}&\sigma_r\hat{n}_r+\tau_{rz}\hat{n}_l={}^{\hat{n}}\bar{\tau}_r\\ &\tau_{rz}\hat{n}_r+\sigma_z\hat{n}_z={}^{\hat{n}}\bar{\tau}_z\end{aligned}\quad (r,\ z)\ \text{on}\ \Gamma \tag{6}$$

where n is the unit outward normal to the boundary Γ and ${}^{\hat{n}}\tau_r$ and ${}^{\hat{n}}\tau_z$ are the externally applied r and z traction components to the boundary Γ.

In the weak Galerkin FE formulation, residual functions exist for lack of satisfaction of the domain and boundary equilibrium equations :

$$\{R_\Omega\}=\begin{Bmatrix}\sigma_{r,r}+\frac{1}{r}(\sigma_r-\sigma_\theta)+\tau_{rz,z}+f_r\\ \sigma_{z,z}+\tau_{rz,z}+\frac{1}{r}\tau_{rz}+f_z\end{Bmatrix} \tag{7}$$

$$\{R_\Gamma\}=\begin{Bmatrix}\hat{n}\tau_r-(\sigma_r\hat{n}_r+\tau_{rz}\hat{n}_z)\\ \hat{n}\tau_z-(\tau_{rz}\hat{n}_r+\sigma_z\hat{n}_z)\end{Bmatrix} \tag{8}$$

The weighted residual statement enforces these error functions to be zero in a weighted integral sense over the domain and on the boundary Γ :

$$\begin{aligned}&\oint_\Gamma N_i(R_\Gamma)\,d\Gamma+\int_\Omega N_i\{R_\Omega\}\,d\Omega=0,\\ &(i=1,\ 2,\ \cdots,\ N)\end{aligned} \tag{9}$$

Here, N is the total number of nodes and N_i is the weighting function associated with node i. The weighting function N_i is given by a piecewise combination of the element interpolating polynomials associated with node i used to interpolate the element displacement field from unknown nodal displacements. For this reason, it is more convenient to express Eq. (9) at the element level :

$$\begin{aligned}&\sum_{e=1}^{M}\Big\{\oint_{\Gamma^e}N_i^e\{R_\Gamma^e\}\,d\Gamma+\int_{\Omega^e}N_i^e\{R_\Omega^e\}\,d\Omega=0,\\ &i=1,\ 2,\ \cdots,\ N\Big\}\end{aligned} \tag{10}$$

where element e, and the summation sign implies the proper assembly of element degrees of freedom (DOF) into the system equations. For axisymmetric elements, one has

$$d\Gamma=2\pi r\,ds \tag{11}$$

$$d\Omega=2\pi r\,dr\,dz \tag{12}$$

Here, ds is the differential path coordinate around the element boundary. Substituting Eqs. (7), (8), (11) and (12) into Eq. (10), and using the divergence theorem to integrate by parts, the higher order terms yield

$$\begin{aligned}&\sum_{e=1}^{M}\Big\{\oint_{S^e}N_i^e\{{}^{\hat{n}}\bar{\tau}^e\}\,r\,ds+\int_{A^e}N_i^e\begin{Bmatrix}f_r^e\\ f_z^e\end{Bmatrix}r\,dr\,dz\\ &=\int_{A^e}\begin{bmatrix}N_{i,r}^e & \left(\frac{1}{r}\right)N_i^e & 0 & N_{i,z}^e\\ 0 & 0 & N_i^e & N_{i,r}^e\end{bmatrix}\begin{Bmatrix}\sigma_r^e\\ \sigma_\theta^e\\ \sigma_z^e\\ \tau_{rz}^e\end{Bmatrix}r\,dr\,dz\\ &i=1,\ 2,\ \cdots,\ N^e\Big\}\end{aligned} \tag{13}$$

The element displacement field is interpolated from nodal values using the element interpolation polynomials N_i^e :

$$\begin{Bmatrix}u^e\\ w^e\end{Bmatrix}=\begin{bmatrix}N_1^e & 0 & \cdots & N_{N_e}^e & 0\\ 0 & N_1^e & \cdots & 0 & N_{N_e}^e\end{bmatrix}$$

$$\begin{Bmatrix} u_1^e \\ w_1^e \\ \vdots \\ \vdots \\ u_{Ne}^e \\ w_{Ne}^e \end{Bmatrix} = [N^e]\{d^e\} \tag{14}$$

Equations (1), (2) and (14) are combined to relate the stress tensor to nodal displacements and substituted into the righthand side of Eq. (13) to obtain the following FE equations for linear axisymmetric isotropic elasticity with initial strains :

$$[K^e]\{d^e\} = \{F_\tau^e\} + \{F_f^e\} + \{F_o^e\} \tag{15}$$

where

$$[K^e] = \int_{A^e} [B^e]^T [D^e][B^e]\, r dr dz \tag{16}$$

$$\{F_\tau^e\} = \oint_{S_e} [N^e]^T \{\hat{n}\tau^e\}\, r ds \tag{17}$$

$$\{F_f^e\} = \int_{A^e} [N^e]^T \{f^e\}\, r dr dz \tag{18}$$

$$\{F_o^e\} = \int_{A^e} [B^e]^T [E^e]\{\varepsilon_0\}\, r dr dz \tag{19}$$

and

$$[B^e] = \begin{bmatrix} N_{1,r}^e & 0 & \cdots & N_{Ne,r}^e & 0 \\ \left(\frac{1}{r}\right)N_{1,r}^e & 0 & \cdots & \left(\frac{1}{r}\right)N_{Ne,r}^e & 0 \\ 0 & N_{1,z}^e & \cdots & 0 & N_{Ne,z}^e \\ N_{1,z}^e & N_{1,r}^e & \cdots & N_{Ne,z}^e & N_{Ne,r}^e \end{bmatrix} \tag{20}$$

The element stiffness matrices and element load vectors are assembled into the system equations. Kinematic boundary conditions are imposed and the equations are factored and solved for nodal displacements. Element strains and stresses are then recovered via Eqs. (1), (2) and (14).

3. Description of Geometry, Material and Loading Condition

The application of FEA to composites requires careful attention to the geometry of the mesh used in analysis and design. In a discontinuous fiber reinforced composite, fiber interaction effects must be important for understanding the deformation evolution in the matrix as well as the overall composite stress-strain behavior except in very low fiber volume fraction cases (Agarwal *et al.*, 1974 and Christman *et al.*, 1989). A 2-D multiple fiber model used to develop the physical concepts is shown in Fig. 1(a) for the aligned fiber geometry.

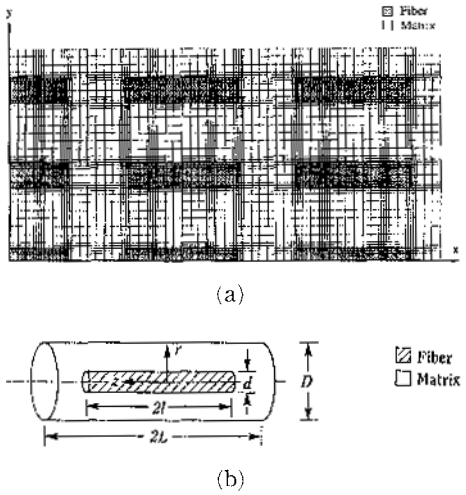

Fig. 1 (a) 2-D multi-fiber model for aligned fiber geometry, (b) Composite RVE containing a single fiber in a cylindrical matrix volume.

On the other hand, an axisymmetric single fiber model corresponding to a 3-D model for the aligned geometry and fiber/fiber interactions can be accounted for by use of cell boundary constraining conditions. In this study, an axisymmetric single fiber representative volume element (RVE) which qualitatively and quantitatively provides the equivalent results as the 3-D model was employed as shown in Fig. 1(b). The RVE is treated as concentric cylinders with diameter D and length $2L$ as shown in Fig. 1(b). The spatial variable for the axial (mechanical loading) direction is z with the coordinate origin at the fiber center, whereas the spatial variable for the radial direction is r. For an FE mesh generation, consequently, a quarter of RVE is needed to analyse due to axisymmetry. FE computations were performed using four noded isoparametric elements. The schematic domain of the composite and the decomposed fiber and matrix is shown in Fig. 2 (a) and (b), respectively.

Material properties selected are for Al 2124 as matrix and SiC whisker as reinforcement. For this system, values used are $E_m = 70\text{GPa}$, $\nu_m = 0.33$

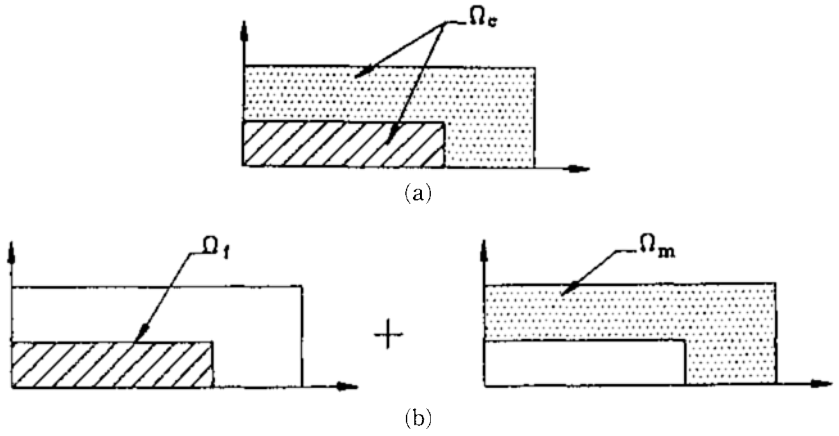

Fig. 2 A schematic of composite domain and the fiber/matrix decomposition process (a) composite domain, (b) decomposed fiber and matrix domains.

and $\alpha_m=2.36\times10^{-5}/K$ for matrix and $E_f=$ 480GPa, $E_f=0.17$ and $\nu_f=4.3\times10^{-6}/K$ for reinforcement (Taya and Arsenalut, 1989, Kim, 1992, Kim, 1994). Here E is Young's modulus, ν is Poisson's ratio and is the CTE. The fiber and matrix materials are assumed to be isotropic, and the elastic constants and CTE values are assumed to be temperature independent. The fiber volume fraction V_f is used as $V_f=0.2$ and the fiber aspect ratio s is used as $s=4$ corresponding to that observed for SiC whiskers in Al alloys (Arsenault and Shi, 1986, Nair and Kim, 1991). Here, fiber volume fraction is not a sensitive factor or function in this study. It was only applied to the case of widely used $V_f=0.2$. The fiber/matrix bond is assumed to be large enough such that no debonding is allowed in keeping with the actual situation in many metal matrix composites (Nair et al., 1985, Kim, 1994). Therefore, slip at the fiber/matrix interface is not allowed in this model. Further, no plastic yielding is allowed, that is, both matrix and fiber deform in a purely elastic manner.

Two cases are evaluated for loading conditions with the same geometry : mechanical loading and thermal loading due to mismatch of CTE between the fiber and matrix. For mechanical loading, a uniform constant composite strain $\varepsilon_c=0.1\%$ is applied on the $z=L$ surface of the RVE. For thermal loading, a uniform temperature difference of $\Delta T=-100K$ as a result of a temperature change (cooling) is applied. Detailed boundary conditions for mechanical and thermal loading are given by Kim (1992).

4. Global Error Estimation

The convergence study, also called the mesh refinement study, is an important and necessary step in FEA. This step, which estimates the discretization error in the solution, is necessary because FE solutions are only numerical approximations. In this section, global error energy as well as local tractions are introduced for the fiber and matrix, respectively. The error approximation technique used here is similar to that given by Zinkiewicz & Zhu (1987). The key difference is that continuous stresses are generated directly by averaging nodal stresses, whereas they impose a weighted residual quality on the stress error estimate.

In the displacement based FE formulations for stress-deformation analysis of solids, the displacement field from element is continuous since C^0 continuity field is assumed. However, the FE stress field, $\{\sigma\}$ is generally discontinuous across inter-element boundaries (Cook *et al.*, 1989). To obtain an improved estimate of the stresses, averaging of the element nodal stresses was employed in this work, i. e.,

$$\{\bar{\sigma}^*\}_n=\frac{1}{K}\sum_{e=1}^{K}\{\hat{\sigma}\}_n^e \tag{21}$$

where $\{\bar{\sigma}^*\}_n$ is the smoothed stress vector at node n. e is the element number sharing node n, K is the total number of elements sharing node n, $\{\hat{\sigma}\}_n$ is the unaveraged stress vector at node n for an element e. Then, the improved stress field in each element e is obtained by interpolating the averaged nodel stress vector $\{\bar{\sigma}^*\}_n$ using the standard FE interpolating polynomials (i. e. shape functions) $[N^e]$:

$$\{\sigma^*\}^e=[N^e]\{\bar{\sigma}^*\}^e \tag{22}$$

where $\{\sigma^*\}_n$ is the improved stress vector at node n. An estimated stress error vector function for the element e is given by

$$e_\sigma^e=\{\sigma^*\}^e-\{\hat{\sigma}\}^e \tag{23}$$

The energy norm of the element stress vector, $\| e_\sigma^e \|$ is given by

$$\| e_\sigma^e \|=\int_{Ve}\{e_\sigma^e\}[e^e]^{-1}\{e_\sigma^e\}dV^e \tag{24}$$

where $[D^e]$ is the element stress-strain matrix. This measure of the error is sometimes referred to as the energy error norm.

The energy norm of the stress error over the entire model for the fiber or for the matrix is given by the square root of the sum of the square of the individual element energy error norms :

$$\| e_\sigma \|_f=\left[\sum_{e=1}^{M_f}\{\| e_\sigma^e \|_f\}^2\right]^{1/2} \tag{25}$$

$$\| e_\sigma \|_m=\left[\sum_{e=1}^{M_m}\{\| e_\sigma^e \|_m\}^2\right]^{1/2} \tag{26}$$

where M is the number of elements and subscript f and m represent fiber and matrix, respectively. The energy norms of the stress error for the fiber and matrix material regions are normalized by the energy norm of the exact stress field for the fiber and matrix regions. The exact energy norms are estimated from the approximate stress solutions in the following manner :

$$[\| \sigma \|_f]^2=[\| \hat{\sigma} \|_f]^2+[\| e_\sigma \|_f]^2 \tag{27}$$

$$[\| \sigma \|_m]^2=[\| \hat{\sigma} \|_m]^2+[\| e_\sigma \|_m]^2 \tag{28}$$

where e f and $\| e_\sigma \|_f$ and $\| e_\sigma \|_m$ are given by Eqs. (25) and (26). Thus,

$$[\| \hat{\sigma} \|_f]^2=\sum_{e=1}^{M_f}[\| \hat{\sigma}^e \|_f]^2 \tag{29}$$

$$[\| \hat{\sigma} \|_m]^2=\sum_{e=1}^{M_m}[\| \hat{\sigma}^e \|_m]^2 \tag{30}$$

Accordingly, normalized percent errors in the energy norm of the error for fiber and matrix are given by

$$E_f=100\left(\frac{\| e_\sigma \|_f}{\| \sigma \|_f}\right) \tag{31}$$

$$E_m=100\left(\frac{\| e_\sigma \|_m}{\| \sigma \|_m}\right) \tag{32}$$

Application of the global energy error norm approach to the fiber reinforced composite material is accomplished by calculating separately the global energy norm for fiber and matrix as in Eqs. (31) and (32). This is because, as previously mentioned, C^0 continuity in the complete stress vector does not exist at the fiber/matrix interface.

5. Local Error Estimation

Although the maximum stress is often used for local convergence, the presence of the singularity at the fiber corner, due to fiber/matrix modulus mismatch and/or CTE mismatch, makes it cumbersome, as can be seen in Fig. 3. The figure shows axial stresses at the fiber corner as a function of mesh size (h=element length at the fiber tip) in Al/SiC for the mechanical loading and the thermal loading, respectively. As can be seen in Fig. 3, convergence is not obtained. Consequently, some other local quantities such as interfacial values near the apex would be another choice.

In FEA, component stresses are calculated for each element at its integration points (or Gauss points). The stress values are then extrapolated to the nearest node using element shape functions,

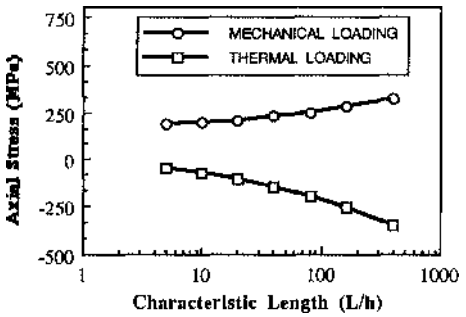

Fig. 3 Axial stresses at the apex of the fiber as a function of mesh size for the mechanical and thermal loading.

resulting in a nodal component stress for that node due to that element. At a node shared by two elements, therefore, we have two nodal stress values, one from each element. In general, the nodal stresses in the entire model are averaged by the stress contributions from all elements shared by a particular node.

This averaging scheme is acceptable in most cases, but there are some instances where the scheme becomes quite inappropriate, as *discontinuities* in element stiffness. In this case, stress averaging does not make sense at nodes shared by elements with different material properties or different geometric properties. In such case, the calculation processed by elements of the same material or geometric property individually can be a good choice. Therefore, geometric or material mismatch at the interface can be evaluated. In this study, this mismatch scheme has been employed and evaluated in detail. Accordingly, the traction difference across the fiber/matrix interface as can be seen in Eq. (33) is used to ensure mesh convergence because the traction must be compatible at interface.

$$\Delta T_n = T_n^f - T_n^m \tag{33}$$

In other words, the traction of fiber T_n^f has to be compatible with that of matrix T_n^m at the interfacial node n. Therefore, the traction differential ΔT_n (see Eq. (33)) at interface should tend to zero as DOF increases.

6. Finite Element Mesh Refinement Strategy

Stress contour results of mechanical loading are shown in Figs. 4(a) and (b) for axial and radial components, respectively. In the same fashion, the results of thermal loading are shown in Figs. 5(a) and (b) for axial and radial components, respectively. As shown in these figures, significant thermal stresses can develop in a short fiber reinforced composite due to CTE mismatch. Furthermore, the thermal axial stress contours vary in the similar manner functionally as those obtained in the mechanical loading. In all cases, it is clear that high local stress gradient regions are near the fiber/matrix interface. Far from the fiber/matrix interface, stresses are fairly uniform. Therefore, the interface region must be discretized as finely as possible so as to achieve convergence efficiently.

The standard h-based mesh discretization pro-

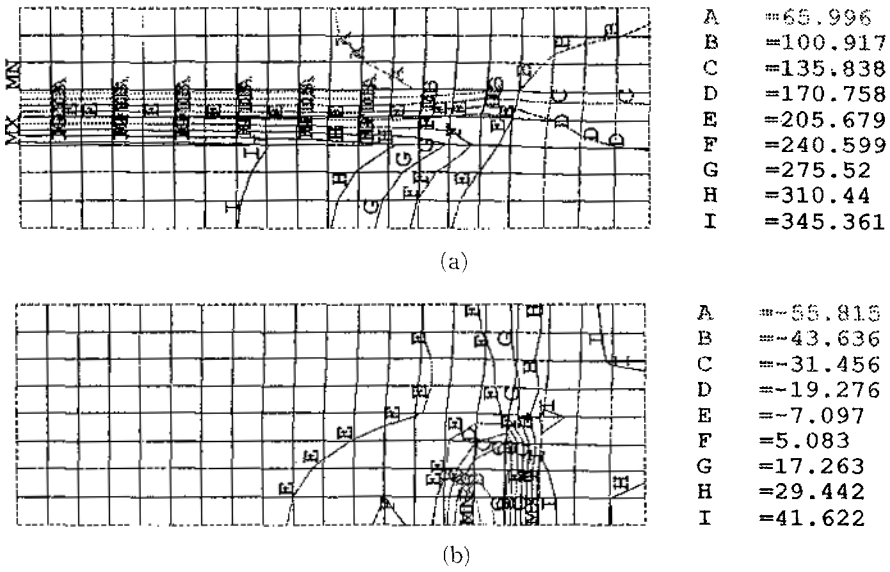

Fig. 4 Stress contours in SI unit (MPa) for mechanical loading (ε_c=0.1%): (a) Axial stresses, (b) Radial stresses.

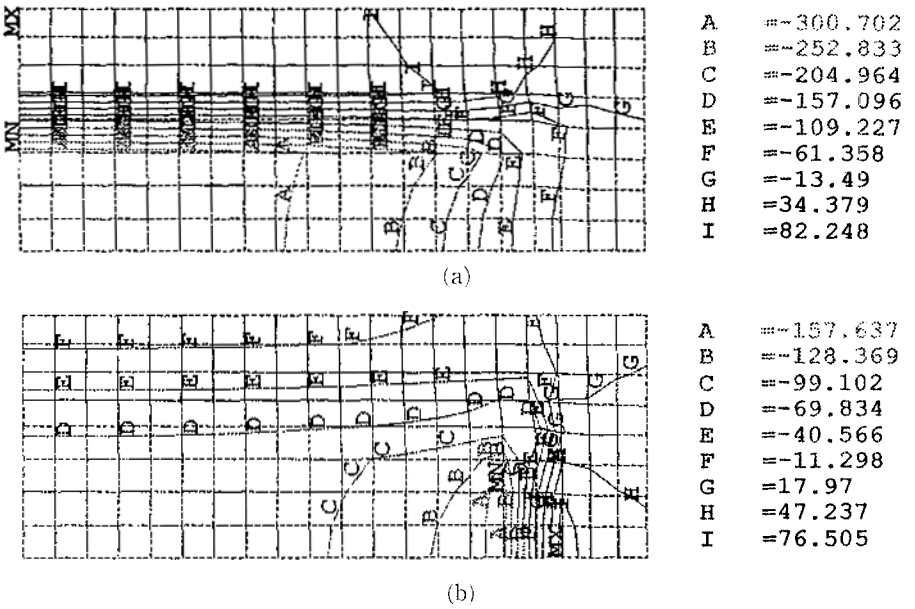

Fig. 5 Stress contours in SI unit (MPa) for thermal loading ($\Delta T = -100K$): (a) Axial stresses, (b) Radial stresses.

cedure involves mesh refinement with unit or near-unit element aspect ratios. Fig. 6(a) shows the regular element (RE) type uniform mesh pattern generated by the ANSYS (Konke, 1989) automatic free mesh generator and Fig. 6(b) shows the elongated element (EE) type mesh pattern. The use of these EE type meshes near the fiber/matrix interface substantially reduces the DOF. Note that the refinement of the EE type mesh is extended to the cell boundaries in both the axial and radial directions. This was done for two reasons: firstly, it simplifies greatly mesh generation, and secondly, a close examination of stress analysis results reveals significant stress gradients in these extended regions compared to the uniform mesh region.

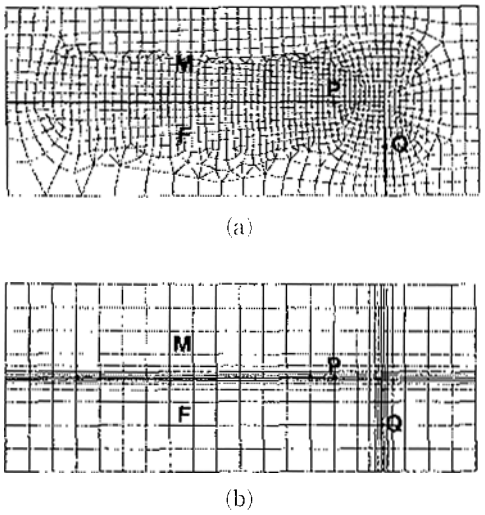

Fig. 6 Typical mesh patterns discretized by (a) a unit or near unit element aspect ratio (RE), (b) an elongated element aspect ratio near the fiber/matrix interface (EE), respectively. M indicates matrix and F indicates Fiber.

7. Results and Discussion

7.1 Global convergence

The error in the energy norm was evaluated separately for each material as describes above. The global error energy norms used by RE and EE meshes for mechanical loading are shown in Figs. 7(a) and (b), respectively. It is clear that energy norm of the error drops quickly and converges to a small but finite error in the energy norm as shown in Fig. 7. For the case of the RE based meshes, the limiting values with about 2500 DOFs are approximately 3% and 5% for the fiber and matrix, respectively. However, for the EE

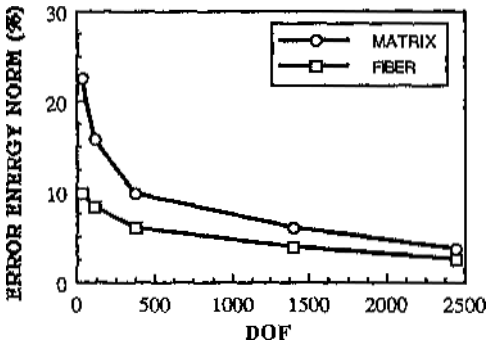

(a)

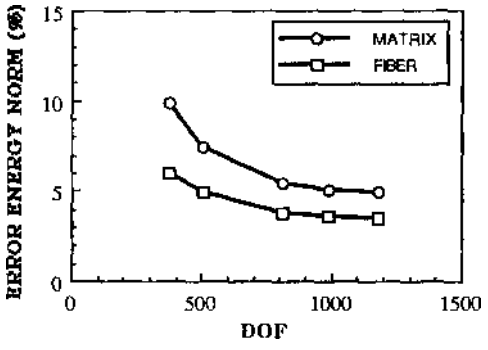

(b)

Fig. 7 Results of global convergence computed by error energy norm approach for the mechanical loading: (a) Convergence for RE type meshes, (b) Convergence for EE type meshes.

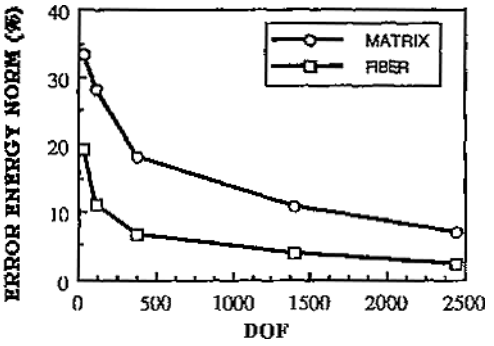

(a)

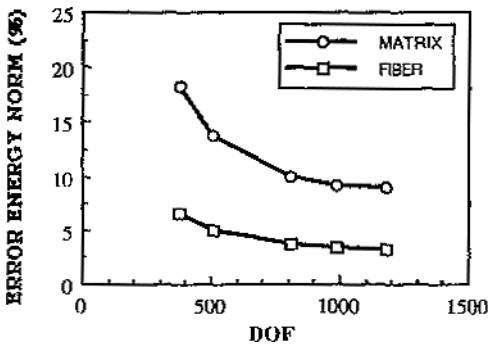

(b)

Fig. 8 Results of global convergence computed by error energy norm approach for the thermal loading: (a) Convergence for RE type meshes, (b) Convergence for EE type meshes.

based meshes, the global error energy norms converge to approximately 4% and 6% for the fiber and matrix, respectively when DOF is 1178 which is a functionally similar result compared to that of RE meshes. Figures 8(a) and (b) show the error energy norms for the case of thermal loading. For both RE and EE based meshes, as can be seen in Figs. 7 and 8, the tendency between the mechanical loading and the thermal loading does not show significant differences.

Although the EE based meshes converge to a functionally similar error in the energy norm to the RE based meshes, the convergence rate for the EE meshes is much faster than for the RE based mesh in both mechanical loading and thermal loading cases. For example, the asymptotic 5% error in energy norm in the fiber is achieved for the EE based meshes with only 500 DOF, whereas approximately 1000 DOF are needed for the RE based mesh to obtain a similar global percent error in energy norm of the fiber for both mechanical and thermal loading cases.

This result is expected since for the same number of DOF, the characteristic element size at and near the interface for the RE type mesh is much larger than that of the EE type mesh. Note that the lack of stress gradients in the fiber direction at the fiber/matrix interface implies that the characteristic element length of the EE elements is given by the element length in the direction perpendicular to the fiber. Thus, comparable accuracy can be achieved using significantly fewer, high aspect ratio EE elements which have the same characteristic element length as an RE mesh. However, as the aspect ratio of the EE elements increases, the stiffness matrix becomes increasingly ill-condi-

tioned (Cook et al., 1989) which introduces numerical error in the solution phase. This is reflected by the higher converged percent error in global energy norm for the EE meshes.

Generally, it is expected that the error as measured by the global error energy norm will converge to zero as the mesh is refined. However, in the discontinuous composite system, stress singularities exist at the fiber/matrix corners which significantly reduce the convergence rate in the global energy norm of the stress error for h-based mesh refinement. Thus, it is unrealistic to demand convergence of the global energy norm to an arbitrary small value for problems involving stress singularities.

7.2 Local convergence

A more dramatic difference between the EE and RE mesh cases can be seen in the local convergence results. For assessing local convergence two points at the interface near the singularity are chosen. One is taken as the near point in the r direction (Point P in Fig. 6(a)) and the other is taken as the near point in the z direction (Point Q in Fig. 6(a)). Then, the normal traction was calculated in each material. The results for mechanical loading are shown in Figs. 9(a) and (b) which reveal a considerably more rapid convergence for the traction compatibility to the EE mesh when compared to the RE mesh case. Thermal loading results are shown in Figs. 10(a) and (b), which also give similar rapid convergence. Accordingly, it is clear that elongated meshes at the fiber/matrix interface yield substantially superior convergence in a local sense. Note that while this simple mesh refinement scheme results in elongated elements at the fiber/matrix interface away from the singularity corner, nearly square elements are generated in the vicinity of the singularity corner.

It is important to realize that convergence to the exact solution at each and every point in the domain is never guaranteed in the FEA. Convergence theorems, such as the *fundamental convergence theorem,* are only able to ensure convergence to the exact solution in the global energy sense (Strang and Fix, 1973). Thus, it is theoretically possible for the solution to converge to the exact solutions as measured by the global energy error norm, but it may fail to converge to the exact solution at each and every point in the domain. Nevertheless, it has been noted that for physically well-posed problems, pointwise convergence does occur if the solution converges in the global energy (Burnett, 1988) which is well documented in the literature (Burnett, 1988, Cook *et al.,* 1989, Kelly *et al.,* 1983, Zhu and Zinkiewicz, 1990). A common misconception is that this superconvergent effect of the pointwise error implies that the relative pointwise error is bounded by the relative error in the energy norm. In general, the convergence *rate* in the pointwise error exceeds the convergence *rate* in the energy norm, but no definitive correlation of the relative pointwise errors to the relative error in energy norm has been offered. Furthermore, the standard convergence theorems in the literature are based

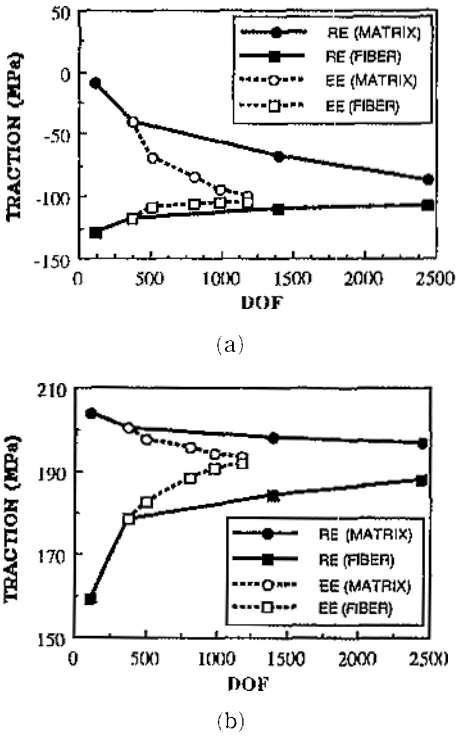

Fig. 9 Results of local convergence computed by traction differential approach for the mechanical loading: (a) Radial stress at point P, (b) Axial stress at point Q.

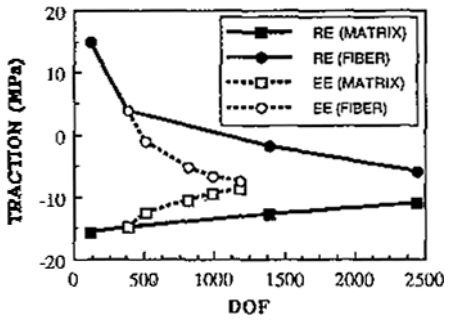

(a)

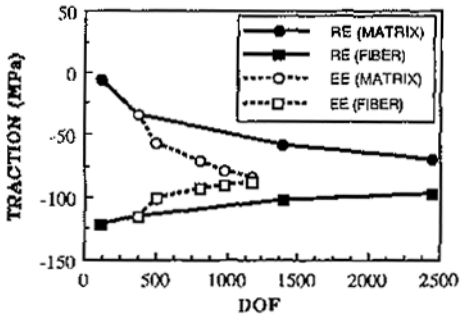

(b)

Fig. 10 Results of local convergence computed by traction differential approach for the thermal loading: (a) Radial stress at point P, (b) Axial stress at point Q.

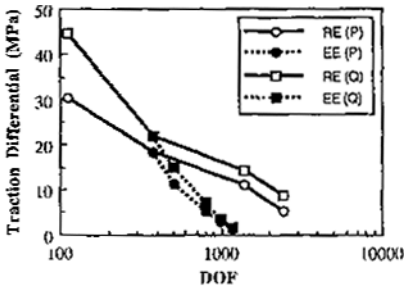

(a)

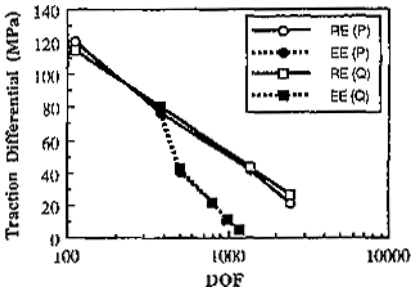

(b)

Fig. 11 Results of local convergence computed by traction differential approach as a function of logarithmic DOF for the axial stress at point Q. : (a) mechanical loading, (b) thermal loading.

on the assumption that the exact solution is "sufficiently smooth" and bounded, and are therefore not strictly applicable to problems in which theoretical singularities exist. It would seem that for such problems, local convergence at points near the singularity can be achieved despite a lack of complete convergence in the global error energy norm due to the singularity. Figures 9 and 10 demonstrate convergence of the traction at specific points for the EE based mesh which imply a significantly smaller relative error in the traction than the 5-6% global error energy norm of Figs. 7(b) and 8(b). The implication is that the global error in energy norm alone is not a sufficient measure of solution convergence. A combination of both global and local error estimates is desirable, especially for problems which admit singularities

Figures 11(a) and (b) show the differential of normal traction as a function of logarithmic DOF the in case of the mechanical and thermal axial loading, respectively. The results show a considerably more rapid convergence for the traction compatibility to the EE mesh when compared to the RE mesh case.

Figures 12(a) and (b) show the logarithmic differential of normal traction as a function of "logarithmic characteristic element length (normalized by a physical length), L/h" in the case of the mechanical and thermal axial loading, respectively. Here, characteristic element length represents a normalized value of the RVE length in axial direction by the element length. The results show again a considerably more rapid convergence for the traction compatibility to the EE mesh when compared to the RE mesh case.

Hence, it is found why EE meshes are better than RE meshes for convergence. An important implication of the FE preprocessing having singularities points out that the key role to obtain the computational efficiency is shortening characteris-

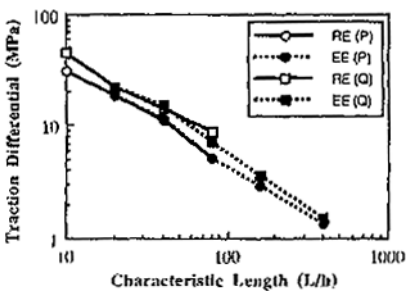

(a)

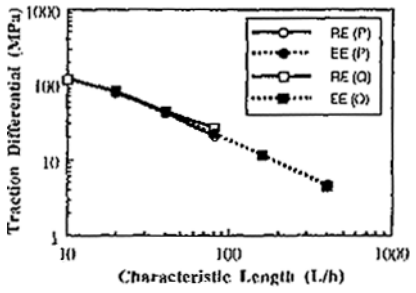

(b)

Fig. 12 Results of local convergence computed by logarithmic differential of normal traction as a function of logarithmic characteristic length (L/h) for the axial stress at point Q. : (a) mechanical loading, (b) thermal loading.

tic element length as shown by the comparison of Figs. 9 and 10 with Figs. 11 and 12. As a result, Figs. 9 and 10 demonstrate the strong statement for computational efficiency while Figs. 11 and 12 demonstrate that there is nothing really magical about the results.

8. Conclusions

A procedure based on the calculation of a new approach using traction differentials at the fiber/matrix interface to ensure global and local convergence has been proposed. The mesh refinement strategy is intended to the h-based generalized approach using the irregular element at the fiber/matrix interface, which yields significantly different patterns compared to the regular mesh patterns. This difference has a critical bearing on the analysis and design implementing FEA. On the strategy, global and local error estimation techniques with a simple h-based mesh refinement are suggested based on map mesh generation techniques for the application to discontinuous, or short fiber reinforced composite materials. The global error estimation technique is based on the total error in the energy norm, calculated separately for each material, and the local error estimation method is based on the fiber/matrix interfacial traction compatibility criterion. Results show that the proposed mesh refinement approach offers a superior convergence rate when compared to h-based automatically refined meshes with near unity aspect ratio elements over this problem domain. This method is also simple to be programmed in an automatic map mesh generator and can lead to results with a high degree of accuracy with a minimum DOF mesh.

Acknowledgement

This work was supported by the 1996 Jeonju university research fund.

References

Agarwal, B. D., Lifsitz, J. M. and Broutman, L. J., 1974, "Elastic-Plastic Finite Element Analysis of Short Fiber Composites," *Fiber Science and Technology*, Vol. 7, pp. 45~62.

Ainsworth, M., Xhu, J. Z., Craig, A. W. and Zinkiewicz, O. C., 1989, "Analysis of the Zinkiewicz-Zuh a-Posteriori Error Estimator in the Finite Element Method," *International Journal for Numerical Methods in Engineering*, Vol. 28, pp. 2161~2174.

Arsenault, R. J. and Shi, N., 1986, "Dislocation Generation Due to Differences between the Coefficients of Thermal Expansion," *Materials Science and Engineering*, Vol. 81, pp. 175~187.

Babuska, I. and Miller, A., 1984, "The Post -processing Approach in the Finite Element Method - Part III: A-Posteriori Error Estimates and adaptive Mesh Selection," *International Journal for Numerical Methods in Engineering*, Vol. 20, pp. 2311~2324.

Babuska, I. and Rheinboldt, W. C., 1978, "A -Posteriori Error Estimations for the Finite Element Method," *International Journal for*

Numerical Methods in Engineering, Vol. 12, pp. 1597~1615.

Babuska, I., Zinkiewicz, O. C., Gago, J. P. and Oliverira, E. R. A., 1986, *Accuracy Estimates and Adaptive Refinements in Finite Element Computations,* John Wiley and Sons, New York.

Burnett, D. S., 1988, : *Finite Element Analysis : From Concept to Applications,* Addison-Wesley, Reading, MA.

Christman, T., Needleman, A. and Suresh, S, 1989, "An Experimental and Numerical Study of Deformation in Metal-Ceramic Composites," *Acta Metallurgica,* Vol. 37, No. 11, pp. 3029~3050.

Cook, R. D., Malkua, D. S. and Plesha, M. E., 1989, *Concept and Applications of Finite Element Analysis,* John Wiley and Sons, Third Edition, New York, pp. 163~295.

Gago, J. P., Kelly, D. W., Zinkiewicz, O. C. and Babuska, I., 1983, "A-Posteriori Error Analysis and Adaptive Processes in the Finite Element Method: Part II, Adaptive Mesh Refinement," *International Journal for Numerical Methods in Engineering,* Vol. 19, pp. 1621~1656.

Grosse, I. R., Katragadda, P. and Benoit, J., 1992, "An Adaptive Accuracy Based a-Posteriori Error Estimator," *Finite Elements in Analysis and Design,* Vol. 12, No. 1, pp. 75~90.

Kelly, D. W., Gago, J. P., Zinkiewicz, O. C. and Babuska, I., 1983, "A-Posteriori Error Analysis and Adaptive Processes in the Finite Element Method: Part I, Error Analysis," *International Journal for Numerical Methods in Engineering,* Vol. 19, pp. 1593~1617.

Kim, H. G., 1992, "Micromechanics of Deformation in Short Fiber or Whisker Reinforced Metal Matrix Composites," Ph. D Dissertation, Department of Mechanical Engineering, University of Massachusetts, Amherst, MA.

Kim, H. G., 1994, "Stress Transfer in Shear Deformable Discontinuous Composites," KSME Journal, Vol. 8, No. 4, pp. 475~484.

Kohnke, P. C., 1989, *ANSYS Theoretical Manual, 5th Edition,* Swanson Analysis Systems Inc., Houston, PA.

Nair, S. V. and Kim, H. G., 1991, "Thermal Residual Stress Effects on Constitutive Response of a Short Fiber or Whisker Reinforced Metal Matrix Composite," *Scripta Metallurgica,* Vol. 25, No. 10, pp. 2359~2364.

Nair, S. V., Tien, J. K. and Bates, R. C., 1985, "SiC-Reinforced Aluminum Metal Matrix Composites," *International Metals Review,* Vol. 30, No. 6, pp. 275~290.

Ohtsubo, H. and Kitamura, M., 1990, "Element by Element *A-Posteriori* Error Estimation and Improvement of Stress Solutions for Two-Dimensional Elastic Problems," *International Journal for Numerical Methods in Engineering,* Vol. 29, pp. 223~244.

Rheinboldt, W. C., 1985, "Error Estimates for Nonlinear Finite Element Computations," *Computers and Structures,* Vol. 20, No. 1, pp. 91~98.

Shephard, M. S., 1979, "Finite Element Grid Optimization with Interactive Computer Graphics," Ph. D Thesis, Department of Structional Engineering, Cornell University, NY.

Strang, G. and Fix, G. J., 1973, *An Analysis of the Finite Element Method,* Prentice-Hall, Englewood Cliffs, NJ.

Taya, M. and Arsenault, R. J., 1989, *Metal Matrix Composites, Thermomechanical Behavior,* Pergamon Press, NY.

Thatcher, R. W., 1982, "Assessing the Error in a Finite Element Solution," IEEE Transactions on Microwave Theory and Techniques, Vol. MTT-30, No. 6, pp. 911-915.

Zinkiewicz, O. C. and Zhu, Z., 1987, "A Simple Error Estimator and Adaptive Procedure for Practical Engineering Analysis," *International Journal for Numerical Methods in Engineering,* Vol. 24, pp. 337~357.

Zhu, Z. and Zinkiewicz, O. C., 1990, "Superconvergence Recovery Technique and a-Posteriori Error Estimators," *International Journal for Numerical Methods in Engineering,* Vol. 30, pp. 1321~1339.